Electroosmosis Based Novel Treatment Approach for Cerebral Edema

Teng Wang, Svein Kleiven, and Xiaogai Li

Abstract*—*Objective: **Cerebral edema characterized as an abnormal accumulation of interstitial fluid has not been treated effectively. We propose a novel edema treatment approach to drive edematous fluid out of the brain by direct current utilizing brain tissue's electroosmotic property.** ***Methods:*** **A finite element (FE) head model is developed and employed to assess the feasibility of the approach. First, the capacity of the model for electric field prediction is validated against human experiments. Second, two electrode configurations (S and D-montage) are designed to evaluate the distribution of the electric field, electroosmotic flow (EOF), current density, and temperature across the brain under an applied direct current.** ***Results:*** **The S-montage is shown to induce an average EOF velocity of 7e-4 mm/s underneath the anode by a voltage of 15 V, and the D-montage induces a velocity of 9e-4 mm/s by a voltage of 5 V. Meanwhile, the brain temperature in both configurations is below 38 °C, which is within the safety range. Further, the magnitude of EOF is proportional to the electric field, and the EOF direction follows the current flow from anode to cathode. The EOF velocity in the white matter is significantly higher than that in the gray matter under the anode where the fluid is to be drawn out.** ***Conclusion:*** **The proposed electroosmosis based approach allows alleviating brain edema within the critical time window by direct current.** ***Significance:*** **The approach may be further developed as a new treatment solely or as a complement to existing conventional treatments of edema.**

***Index Terms*—Cerebral edema, Electroosmotic flow, Electric field, FE head model.**

I. Introduction

CEREBRAL edema is defined as the accumulation of water in extracellular and intracellular spaces, leading to high morbidity and mortality [1], [2]. Among a variety of pathogenic factors, traumatic brain injuries (TBIs) constitute the primary cause for brain swelling that could also lead to other serious complications, especially in younger victims [3], [4]. Moreover, the increased water content in extracellular space may result in increased intracranial pressure (ICP) with potentially deleterious effects unless treated effectively. Current treatments for cerebral edema are limited and mainly to ameliorate the outcome of brain swelling [1]. Osmotherapy has been regarded as the most useful pharmacologic therapy to draw water out of the brain into the vascular compartment by creating an osmotic gradient between the brain and the blood system. This is accomplished by intravenous administration of osmotic agents, such as mannitol and hypertonic saline, resulting in high serum osmolality to shift excess water from the brain into intravascular space. However, this approach may cause side effects such as renal failure and decreased cerebral perfusion [2], [5]. For the most severe brain swelling, decompressive craniectomy (DC) surgery is often considered a last resort to reduce ICP. However, the severe stretching of brain tissue at both the inner brain and bony skull edges in patients who underwent DC surgery may contribute to unfavorable outcomes [6], [7]. Thus, the treatment of cerebral edema is still an arduous task.

Therapeutic methods utilizing external electric fields have been used extensively to treat neurological and psychological disorders during the last decades. For example, transcranial direct current stimulation (tDCS) is used to modulate cortical excitability with weak direct current [8]–[10]. Electrophoresis has wide applications in pharmacologic therapy based on the property of the directional movement of charged particles under an electric field, such as brain iontophoresis [11] and transnasal delivery of the charged peptide [12]. Electroosmotic flow (EOF), defined as fluid flow from one area to another under an electric field, is often neglected in the above applications, which may be due to the difficulty in observing or separating EOF from other induced flows. Electric field has been used to induce electrokinetic transport in brain tissue based on electrophoresis and electroosmosis [13], [14].

EOF in a porous matrix is bulk fluid flow under an electric field due to the electrical double layer (EDL) characterized by zeta-potential [15]. Brain tissue has a zeta-potential [15], is conductive, and the brain extracellular fluid is an electrolyte solution [16]. Thus, the fluid in the extracellular space can flow from one area to another under an electric field according to the electroosmotic principle. EOF often co-occurs with electrophoresis in drug delivery, as shown in the iontophoretic delivery experiment [11]. Several applications have been developed based on brain tissue's electroosmotic property. For example, electroosmotic sampling is used to pull extracellular fluid from living tissue into a capillary with an applied electric

Manuscript received August 27, 2020; revised November 13, 2020 and December 13, 2020; accepted December 14, 2020. Date of publication December 18, 2020; date of current version August 20, 2021. The work of Teng Wang was supported in part by the China Scholarship Council and in part by a VFT-1 fas 0 fund from KTH Innovation (project title: Edema Treatment) at the KTH Royal Institute of Technology, Sweden. *(Corresponding author: Teng Wang.)*

Teng Wang is with the Department of Biomedical Engineering and Health Systems, KTH Royal Institute of Technology, 141 52 Huddinge, Sweden (e-mail: tenwan@kth.se).

Svein Kleiven and Xiaogai Li are with the Department of Biomedical Engineering and Health Systems, KTH Royal Institute of Technology, Sweden.

Digital Object Identifier 10.1109/TBME.2020.3045916

field [17]–[20], suggesting that the induced fluid always follows the electric current pathways from anode to cathode. In clinical applications, EOF has been observed in electrochemical treatment of liver tumors under direct current, in which a net flow of water is moved from anode to cathode [21]. Moreover, the zeta-potential and tortuosity of the rat brain has been measured based on the combination of electrophoresis and EOF, in which the EOF velocity was quantified [22], [23].

The above studies provide convincing evidence for the electroosmotic properties of the brain, especially the pioneer works by Weber's group have shown the capability of inducing fluid flow in brain tissue cultures [18]–[20], [24] and in rat brain [13], [14] based on electroosmosis. However, the intention of utilizing electroosmosis for brain edema treatment has not been explored to date. Thus, the aim of this study is to investigate the effect of direct current on fluid transport across the brain and the feasibility of inducing bulk fluid flow with an applied electric field to mitigate cerebral edema.

II. Methods

A. Finite Element Head Model

A finite element (FE) head model is developed based on the ICBM 152 atlas, including T1W, T2W, and probability maps [25]. The segmentation is performed using the Expectation-Maximization (EM) algorithm together with the spatial information provided by the probability maps, which is implemented in Slicer 3D [26]. The FE mesh is then generated by converting segmented voxels into hexahedral elements using a smoothed-voxel algorithm presented in an earlier study [27]. The resultant mesh consists of 3.45 million hexahedral elements with an element size of about 1 mm. The final FE model is composed of the scalp, cortical bone, cancellous bone, dura mater, cerebrospinal fluid (CSF), gray matter (GM), white matter (WM), and the ventricular system (Fig. 1(a)). The model is then imported into COMSOL Multiphysics (Comsol Multiphysics, 2017, v5.3a) for numerical simulations.

The electrode configuration of the S-montage consists of an anode pad (5 cm $\times$ 5 cm) located at the side of the head and a cathode pad (3 cm $\times$ 10 cm) located at the top (Fig. 1(b)). The D-montage has a similar electrode placement, except the scalp and skull underneath the anode are removed, resulting in direct contact between the inner surface of the anode and the dura mater (Fig. 1(c)). Note in both configurations, the cathode is designed to be near the subarachnoid space (SAS) to facilitate the extra fluid to be absorbed into SAS together with CSF, and the anode is close to the brain area where extra tissue fluid is intended to be drawn out. In both configurations, both the anode and cathode include a metal electrode and a saline-soaked sponge.

B. Modeling of Electroosmotic Flow

The brain tissue has a zeta-potential [15], is conductive, and the brain extracellular fluid is an electrolyte solution [16]. The stationary cells and other components of the extracellular matrix build the porous structure with narrow channels filled with extracellular fluid. Due to the negatively charged phospholipid cell membranes, the cations in the extracellular fluid are attracted and

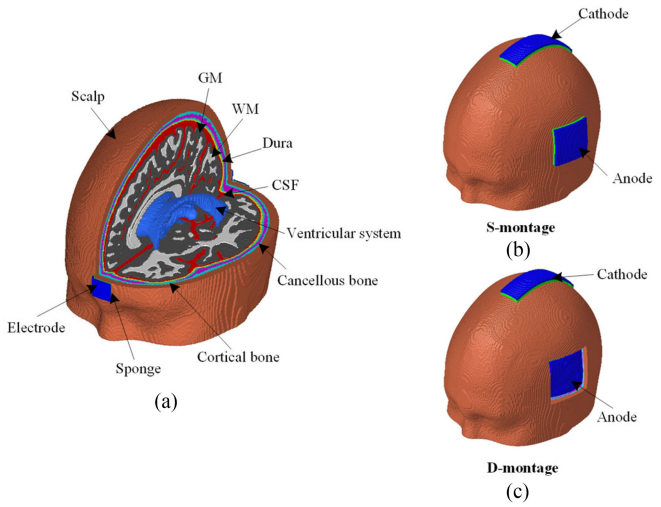

Fig. 1. (a) FE head model with anatomical details including the scalp, cortical bone, cancellous bone, dura mater, CSF, GM, WM, and ventricular system. The head model is validated with an anode located at mid-forehead and a cathode located at occiput. (b) S-montage: The anode pad in contact with the scalp surface is placed on the side of the head, and the cathode pad is placed on the top of the head. (c) D-montage: The placement is similar to that in S-montage, except that the anode is in direct contact with the dura mater.

distributed close to the surface, forming the EDL, which consists of a stern layer and a diffuse layer [16], [28]. Under an externally applied electric field, the cations are driven by electrical force through the micro-channels in the extracellular space, resulting in adjacent fluid flow together by viscous drag force [16], [22]. The EOF velocity (ν) is governed by Helmholtz–Smoluchowski approximation:

$$\nu = -\frac{\varepsilon_r \varepsilon_0 \zeta E}{\eta} \tag{1}$$

where ν is the EOF velocity, E is the electric field, ζ represents the zeta-potential of brain tissue (-22.8 mV) [22], ε_r is the relative permittivity of the extracellular solution, ε_0 is the vacuum permittivity (8.85e-12 F/m), and η is the viscosity of the extracellular solution at average normal body temperature. Following the experiments of zeta-potential measurement in rat brains [22], [23], ε_r and η of water are used here, which are set to 84.6 and 6.4e-4 Pa•s, respectively [29].

C. Modeling of Electric field and Temperature

The electric field in the head is obtained by solving Laplace's equation under quasi-stationary conditions:

$$\nabla \cdot (-\sigma \nabla V) = 0 \tag{2}$$

where ∇ represents the gradient vector, V is the electric potential, and σ is the electrical conductivity of the tissue. The electric field, E, is derived from the electric potential as:

$$E = -\nabla V \tag{3}$$

The current density, J, is calculated according to Ohm's law:

$$J = \sigma E \tag{4}$$

TABLE I
ELECTRICAL AND THERMOPHYSICAL PROPERTIES OF HEAD TISSUES

Tissue	Electrical conductivity σ (S/m)	Thermal conductivity κ (W/(m• °C))	Metabolic heat source Q_m (W/m^3)	Blood perfusion rate ω_b (1/s)
Scalp	0.43478	0.39	363	0.00143
Cortical bone	0.0064	0.65	70	0.000143
Cancellous bone	0.02865	0.65	70	0.000143
Dura mater	0.527	0.44	70	0.000143
CSF	1.79	0.61	0	0
GM	0.3334	0.565	16229	0.013289
WM	0.1428	0.503	4517.9	0.0036956
Ventricular system	1.79	0.61	0	0
Electrode	5.99e7	31		
Sponge	1.4	0.3		

The Joule heating from electric energy consumption is considered as the most important factor for increased temperature, which is introduced by a source term $\sigma|\nabla V|^2$. In this study, steady-state simulations are performed to evaluate the temperature variation, in line with brain temperature modeling in previous studies [30], [31]. For living tissue, blood perfusion and metabolic activity also influence heat transfer, which is accounted for by the bio-heat transfer model described by Pennes equation combined with electrical energy:

$$\rho C_p \frac{\partial T}{\partial t} = \nabla(\kappa \nabla T) - \rho_b \omega_b C_b (T - T_b) + Q_m + \sigma|\nabla V|^2 \tag{5}$$

where ρ is the tissue density, C_p is the heat capacity of the tissue, T is the temperature, κ is the thermal conductivity, ρ_b is the blood density, ω_b is the blood perfusion rate, C_b is the heat capacity of the blood, T_b is the arterial blood temperature, and Q_m is the metabolic heat source.

The electrical and thermophysical properties of the head tissues are taken from the literature [22], [30], [32]–[37] as shown in Table I. Note that the WM has shown anisotropic conductivity with larger values along the axonal direction than perpendicular direction [38], which is not accounted for in this study as previous numerical studies show limited effects of anisotropy on the induced electric field [39], [40]. Therefore, isotropic conductivity is used for WM.

A voltage of 15 V is applied to the anode in the S-montage, and 5 V is applied to the anode in the D-montage. The cathode in both montages is set as 0 V, and all other external surfaces of the FE head model are set as insulated. For thermal boundary conditions, the convection of heat from scalp and electrodes to the ambient is accounted by assigning the following heat flux equation to all external boundaries of the head model:

$$q = h(T_{amb} - T) \tag{6}$$

where h represents the heat transfer coefficient (4 W/m^2•°C), and T_{amb} is the external ambient temperature (24 °C). The initial temperature of the electrode and the sponge is assigned to be 24 °C and a normal body temperature of 36.7 °C is assigned to all head components [30], [31], [35].

The simulations are performed on a computer with an Intel(R) Xeon(R) processor (12 cores, 12 threads) and 48 GB of memory, requiring about 15 minutes for each simulation.

D. Model Validation Against Experimental Data

The FE head model is validated against *in vivo* human experimental data of electric field reported earlier [39]. In the experiment, induced voltages on the cortical surface were recorded with implanted electrodes in epilepsy patients under tDCS, based on which electric field was calculated by dividing the two adjacent electrodes's voltage differences with distance [39]. Following the same as in the experiment, the electrode applied to the FE head model comprises an anode pad (2 cm × 2 cm) placed on the midforehead and a cathode pad (2 cm × 2 cm) located at the occiput (Fig. 1(a)). The injected current of 1 mA is applied to the anode, and the cathode is set in contact with the ground. The predicted voltage and electric field from the FE head model at corresponding locations of implanted electrodes as in the experiment are extracted and compared with experimental data. Pearson's correlation coefficient (r) and slope (s) of the fitted line are calculated between model prediction and the experimental measurement.

III. RESULTS

A. Model Validation Performance

The model predicted voltage and electric field are compared with experimental data to verify the prediction accuracy. The voltage decreases by about 20 mV from the frontal cortex to the occipital cortex (Fig. 2(a)). The maximum electric field mainly locates underneath the electrodes at both mid-forehead and occiput lobe (Fig. 2(c)). The correlation coefficients between measured and predicted values are 0.96 for voltage (Fig. 2(b)) and 0.81 for electric field (Fig. 2(d)), respectively, suggesting a reasonable capability of the model to predict the spatial distribution of voltage and the electric field comparing with human experiments reported earlier by Huang *et al.* [39]. Moreover, the slope of the fitted line is 0.88 for voltage and 0.74 for the electric field, showing the head model can reasonably predict the electric field magnitude across the brain.

B. Electric Field Distribution

The electric field distribution across the WM and GM under direct current is evaluated, showing the activated regions mainly locate under and between the electrodes in both configurations. For the S-montage, the maximum electric field is located in the

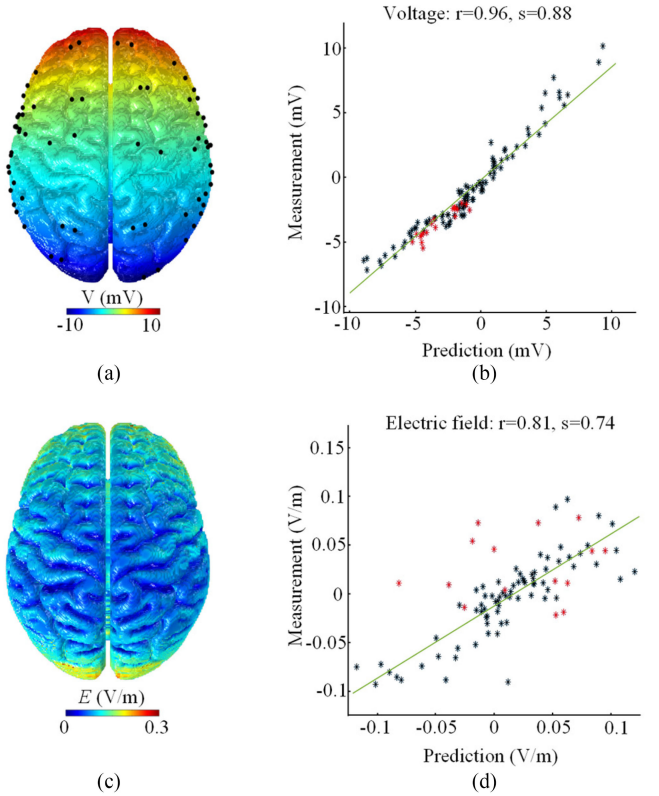

Fig. 2. (a) The voltage distribution across the cortical surface predicted from the head model. The black dots are the locations where the voltage and electric field are evaluated from the head model corresponding to the same locations as the implanted electrodes in the experiment by Huang *et al.* [39] (patient P03). (b) Comparison of measured voltage with predicted values from the head model. (c) The electric field distribution across the cortical surface predicted from the head model. (d) Comparison of the measured electric field with predicted values from the head model. Note in (b) and (d), the black points indicate the measured data from cortical surface electrodes and the red from depth electrodes (mostly targeting hippocampus). The green line represents a linear fitting of the data.

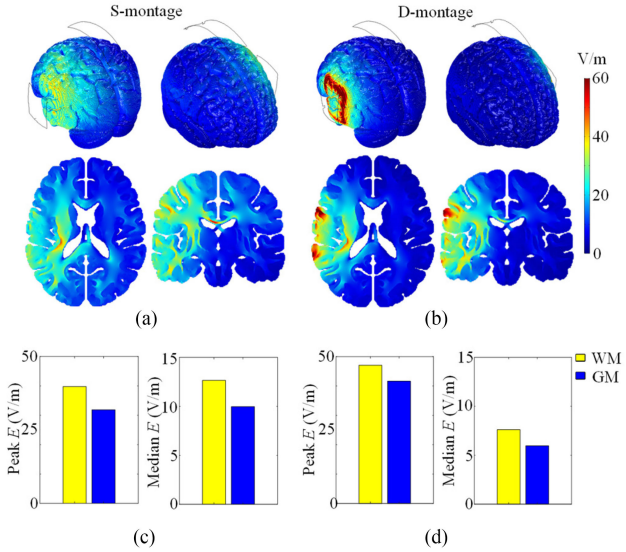

Fig. 3. The distribution of induced electric field (*E*) on the cortical surface and across the WM and GM on representative axial and coronal planes in S-montage (a) and D-montage (b). Peak and median values of the electric field for WM and GM in S-montage (c) and D-montage (d).

WM; and the average electric field in the WM is also higher than GM due to the lower electrical conductivity of the former (Fig. 3(a)). The peak (calculated as the 99th percentile) and median (calculated as the 50th percentile) of the electric field magnitude (Fig. 3(c)) are also higher in WM than in GM. Similarly, the D-montage exhibits higher values of peak and median electric field in the WM (Fig. 3(d)). However, the maximum is observed close to the cortex directly underneath the anode (Fig. 3(b)). Besides, the D-montage induces a higher variation in the electric field between the activated region and the other side of the brain due to the lack of electric current shunting by the scalp and skull underneath the anode.

C. Electroosmotic Flow Across the Brain

The EOF distribution across the brain is calculated under the applied voltage. Similar to the electric field distribution, the EOF distribution of WM and GM exhibits a similar trend in both montage configurations (Fig. 4) as the velocity is proportional to the magnitude of the electric field according to the Helmholtz–Smoluchowski equation (Eq. 1). A faster flow is induced between anode and cathode, especially near the anode, where the average velocity of the WM is higher than that in GM. Further, the induced electric field in the CSF is lower than the brain tissue attributed to the significantly higher electric conductivity of CSF, which consequently leads to lower EOF velocity. Note that an essential condition to induce EOF inside the brain is the narrow channels with charged walls such as the extracellular space. Thus, the electric field mainly induces EOF in the brain parenchyma.

The EOF velocity is further evaluated quantitatively along crosslines in three brain regions, demonstrating a significant variation in EOF velocity among brain regions (Fig. 4). For the S-montage (Fig. 4(a)), the average velocity near the anode is around 7e-4 mm/s, whereas the EOF magnitude in the other hemisphere decreases to 3e-4 mm/s. A similar trend is also observed in D-montage (Fig. 4(b)), in which the average velocity near the anode is around 9e-4 mm/s. As a result, a water particle close to the anode can move approximately 2.52 mm/h along the EOF direction for S-montage, and 3.24 mm/h for the D-montage.

To have a better understanding of EOF flow, the EOF direction is further analyzed (Fig. 5). The EOF is shown to move from anode to cathode, and the polarity of electrode determines the direction of the induced flow. Thus, an anode is to be placed near the edema region to drive the edematous fluid out. Besides, the streamlines suggest that the EOF direction is also affected by the structure and electric conductivity among brain regions. Since the fluid transport in the extracellular space results from the movement of cations by viscous drag, the EOF pathways always follow the direction of current flow from anode to cathode.

D. Current Density and Temperature Distribution

The distribution of induced current density and temperature is evaluated and presented in Fig. 6 and Fig. 7, respectively, as

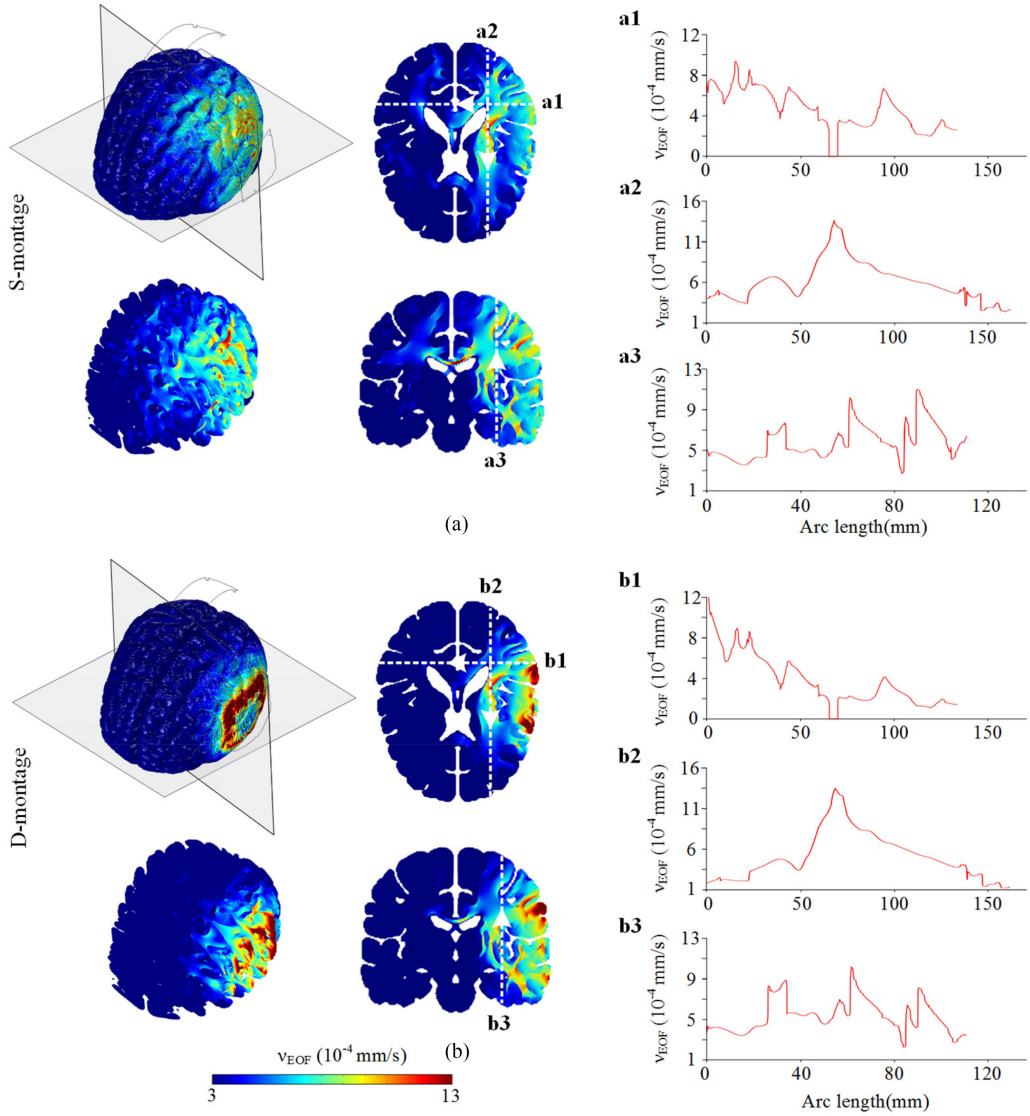

Fig. 4. The distribution of EOF velocity on cortical surface and inside the brain in S-montage (a) and D-montage (b). The EOF velocity along the crosslines in three brain areas on the axial and coronal planes is evaluated quantitatively (S-montage: a1, a2, a3; D-montage: b1, b2, b3).

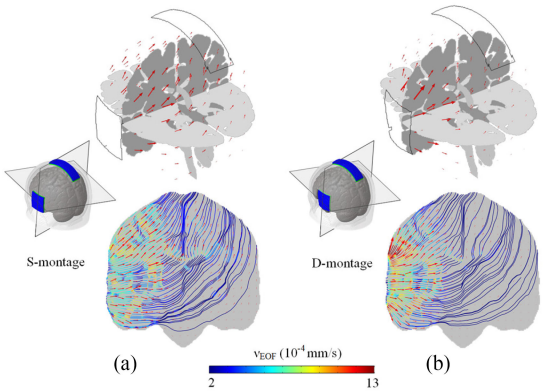

Fig. 5. The direction and pathways of EOF inside the brain in S-montage (a) and D-montage (b). The red arrows show the direction of EOF, and the size of the arrows represents the velocity magnitude. The streamlines represent the EOF pathways, and the color denotes the velocity magnitude.

both factors are suggested to be responsible for brain damage. The highest current density occurs under the anode in both configurations (Fig. 6(a) and (b)). GM has a higher average current density than WM due to its higher conductivity. The peak current density of WM and GM is around 5.7 and 10.6 A/m^2, respectively, in the S-montage (Fig. 6(c)) with an applied voltage of 15 V. The peak value in the D-montage (Fig. 6(d)) is 6.7 A/m^2 for WM and 13.9 A/m^2 for GM with an applied voltage of 5 V. Due to the lack of scalp and skull in the D-montage, the direct current flows through the dura and CSF into the brain directly, resulting in substantially high current density in the GM near the anode.

The temperature distribution with and without applied voltage is investigated for both configurations. For the S-montage, the applied direct voltage exhibits a significant effect on the temperature of the scalp and skull, leading to an increase of maximum temperature from 37.0 °C to 39.2 °C in the whole head, whereas

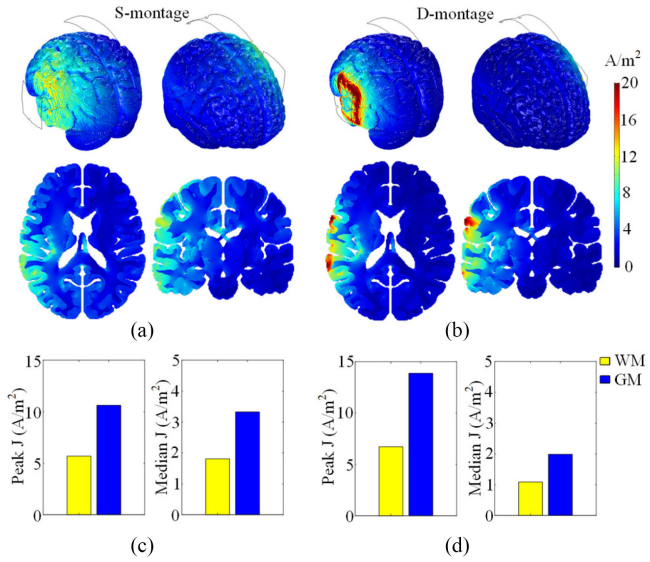

Fig. 6. The distribution of induced current density (J) on the cortical surface and across the WM and GM on the axial and coronal planes in S-montage (a) and D-montage (b). Peak and median values of current density for WM and GM in S-montage (c) and D-montage (d).

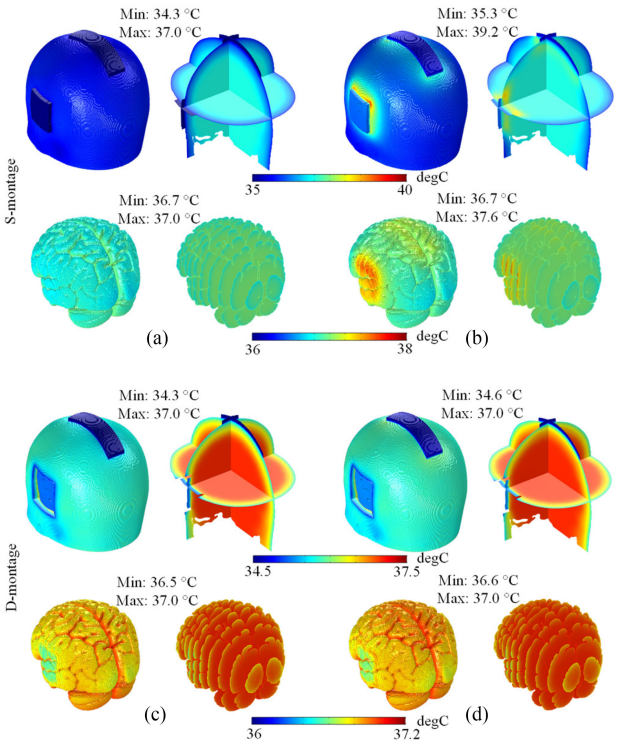

Fig. 7. The temperature variation predicted from the head model. The temperature distribution without externally applied voltage in S-montage (a) and D-montage (c). The temperature variation with an applied voltage of 15 V in S-montage (b) and 5 V in D-montage (d).

the increase of the maximum temperature is only 0.6 °C in the brain (Fig. 7(a) and (b)). For the D-montage, a slight effect is observed across the head model (Fig. 7(c) and (d)) due to the low magnitude of the applied voltage and the convection of heat from the scalp and electrode to the ambient air.

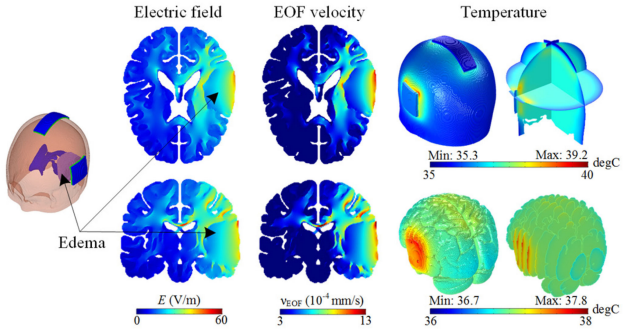

Fig. 8. The predicted electric field, EOF velocity, and temperature from the model with cerebral edema for S-montage.

E. The Effect of Edema on EOF

All the above investigations are on healthy brains, and it would be interesting to study whether and how the induced EOF velocity may vary when cerebral edema presents, as well as how induced temperature may change. Thus, an additional simulation is performed with edema included for the S-montage. Localized edema is assumed underneath the anode with a volume of 87.7 cm^3, as in a representative edema patient [41]. The edema region's electrical conductivity is estimated as 0.3337 S/m (average of edematous WM conductivity of 0.2704 S/m and GM of 0.4053 S/m) based on water content increase quantified in an edema patient [41] that lead to higher conductivity. Since the thermal conductivity is proportional to the percentage of water content [42], the value is set to 0.7 W/(m•°C) for edema region. Moreover, the edema brain will significantly reduce the metabolism and blood perfusion. Thus, the values are set to 10000 W/m^3 for metabolic heat source [43], and 0.006644 1/s for blood perfusion rate in edema region [44].

The distribution of electric field (Fig. 8) inside the edema is slightly lower than that in surrounding regions due to its higher electric conductivity than surrounding healthy tissues. Consequently, the EOF in the edema is lower than surrounding tissues. In contrast, the edema region underneath the anode exhibits a significantly high velocity. The predicted temperature from the model with cerebral edema (Fig. 8) shows a slight variation compared to the results from the model without cerebral edema (Fig. 7(b)). The presence of edema increases the maximum temperature from 37.6 °C to 37.8 °C in the brain. Nevertheless, the temperature in the brain is still within the safety range.

IV. Discussion

This study proposes a novel edema treatment approach to drive edematous fluid out of the swelling brain by applying direct current based on brain tissue's electroosmotic property. To verify the feasibility of the approach, we utilize an anatomically detailed and validated head model, showing the approach allows inducing fluid flow within the critical time window for edema resolution. Meanwhile, the induced current density and temperature increase are within the safety range. Thus, the proposed approach could potentially be developed to a novel therapy that has important clinical implications for both severe and

mild edema treatment by reducing the swelling magnitude and duration in severe edema patients and serve as supplementary for mild edema treatment to complement the limited choice of existing treatments. Especially for severe edema patients with DC surgery, the swelling brain is expanded outside the skull, causing severe axonal stretch, which has been suggested to cause neural injury [6], [7]. The proposed approach may be applied to such patients to reduce the swelling magnitude and duration, thus could potentially improve patients' outcomes. To our knowledge, this is the first study utilizing the brain tissue's electroosmotic property for edema treatment, which could potentially reduce complications in edema patients and improve outcomes.

The underlying mechanisms of the proposed approach are based on brain tissue's electroosmotic property as brain tissue has a substantial amount of dissociated ions in the extracellular space generating an EDL [16]. Based on electroosmosis, a motion of the cations in the EDL can be induced by electric field, which then drags the adjacent fluid, involving charged and neutral particles, along the micro-channels in the extracellular space from the edema region to SAS, where it can be absorbed by superior sagittal sinus underneath the cathode. As the direction of EOF is from anode to cathode, thus, for edema treatment, the anode is to be placed near the edema and cathode near the SAS to facilitate edematous fluid absorption. The simulation results show edematous fluid can be transported from the edema region to SAS at an average velocity of 7e-4 mm/s in S-montage and 9e-4 mm/s in D-montage (Fig. 4) by applying an external electric field. Compared to the interstitial fluid flow with a velocity of approximately 6e-4 mm/s [45], the induced fluid transport can double the fluid flow rate away from the edema region since the EOF always flows along the direction from anode to cathode. In addition, the activated brain region by direct current is mainly located under and between anode and cathode, whereas the hemisphere on the other side shows lower EOF velocity (Fig. 4), indicating that the direct current and the induced fluid transport have only a slight effect on the healthy tissue. Worth mentioning that the direct current also has a limited effect on the CSF circulation, avoiding the CSF into GM underneath the anode under an applied electric field.

According to the Helmholtz–Smoluchowski equation, the magnitude of induced fluid transport is linearly correlated to the electric field. Therefore, the electric field determines the EOF distribution inside the brain. The high correlation coefficient and nearly linear slope of the fitting line between measured and predicted values (Fig. 2) indicate capacity of the FE head model to predict the electric field, which guarantees a similar accuracy of the predicted EOF distribution. As the fluid transport results from the charged ions movements driven by an applied electric field, the EOF direction follows the pathways of current flow, consistent with the findings of Cancel *et al.* [46]. For the current flow, the pathways are mainly affected by electrode configurations, shape, structure, boundary condition, and electric conductivity among different components of the brain [47]. Therefore, the EOF direction can be designed individually based on the edema location by adjusting the electrode configuration.

As the intention of this study is to investigate the feasibility of the proposed approach, healthy head models are employed here. Nevertheless, to have an insight of the effect of edema region on EOF distribution, an additional simulation is performed with edema included for the S-montage. For the FE head model with cerebral edema, because the electrical conductivity of edema region is higher than that in WM and GM, the EOF velocity in the edema region is slightly lower than its surrounding tissue (Fig. 8).

It's important to consider safety issues when applying direct current to the brain, as brain damage has been shown to be caused by multiple factors under an electric field, including current density, temperature variation, voltage drop, power density, and the duration of treatment [48]. In particular, current density is regarded as an important criterion for brain damage. By comparing an FE model predicted current density with measured values in rat experiments, Bikson *et al.* [48] and Liebetanz *et al.* [49] suggest a threshold of 12 A/m^2 for brain damage in human using a rat-to-human scaling factor of 240. Further, brain damage is observed with a 500 μA direct current for 10 minutes, whereas the brain is safe under the same current strength for 3.33 minutes [49]. In the current study, the peak current density in the brain is 10.6 A/m^2 for the S-montage and 13.9 A/m^2 for the D-montage, respectively, which is close to the above threshold. Related to this, *in vivo* experimental studies on cellular level for electroosmotic sampling show current density higher than 100 A/m^2 without visible cell death [50], and the electric field necessary to electroporate a cell is up to 6.7e3 V/m [51]. Considering possible duration effect, when the direct current is applied to the brain for cerebral edema treatment, intermittent treatment may be a reasonable choice to keep the patients safe.

Possible electrochemical reactions at the electrode-tissue interface (i.e., electrode-scalp in S-montage and electrode-dura in D-montage) for the proposed approach should be considered. Especially, side effects of skin sensation and irritation have been reported in tDCS [52] caused by electrochemically produced toxins and electrode dissolution products at the electrode-tissue interface [53]. However, these side effects are often benign and not severe, also can be avoided by preventing direct contact of the electrode and the skin by electrolyte [54]. Similar precautions could be taken when used for edema treatment proposed in this study, e.g., by a thick saline-soaked sponge or conductive gel to provide a buffer with sufficient electrolyte preventing chemicals formed at the electrode surface from reaching the skin or dura. Moreover, since EOF can be used as an intermittent treatment, replacing the electrode and electrolyte sponge timely could minimize or avoid electrochemically produced toxic products reaching the scalp or dura.

In terms of temperature, brain tissue is sensitive to temperature variation and can be damaged or ablated at a sustained temperature over 40 °C [31]. On the other hand, the scalp is usually reported as the most likely component suffering skin burns beneath the electrodes in electrical treatment due to its direct contact with the electrode. The maximum temperature predicted from the current models is below 40 °C, occurring at the scalp surface near the electrode edges. Besides, the temperature in the brain is below 38 °C, indicating that the network function,

cell excitability, as well as blood-brain barrier function of brain tissue, would not be altered by induced temperature variation [31], [35]. Further, sustained brain temperature increases above 40–41 °C may be considered as a threshold for pathological hyperthermia [31], [55], which seems to indicate the brain under a longer duration of 38 °C should not cause damage. Since the joule heat generated by electric current is linearly dependent on current density, the temperature elevation in the brain can be regulated to non-harmful levels by decreasing the applied electric current density.

For electroosmotic sampling, the extracellular fluid is pulled into a fused-silica capillary based on the cations' movement from anode to cathode with an applied direct current [18]–[20]. Besides, the zeta-potential of rat brain is measured by calculating the electrophoretic velocity of fluorescent probes and induced EOF velocity across the hippocampus, which provides the first visualization of EOF in the brain and the methods to quantify the velocity [22]. The material parameters used for calculating EOF velocity within the brain are based on zeta-potential measurement of rat brains [22] due to the lack of experimental data on human brain tissue.

This study verifies the feasibility and safety of the proposed approach using numerical models. Future animal experiments should be performed to further confirm the safety of applied voltage dose for a specific electrode configuration, as well as to further verify the efficiency of this approach in reducing cerebral edema. Weaker direct current is used in tDCS to modulate brain activity which is shown to be safe. Whether or not and how a higher direct current used in this study intended for edema treatment may influence the neuron excitability or network function could be further studied. Nevertheless, as the induced fluid transport under direct current is proportional to the electric field, a lower current density than proposed in the present study could be used despite a lower induced EOF velocity.

V. Conclusion

In conclusion, we propose a novel approach for edema treatment based on electroosmosis by an applied direct current. The feasibility of the novel approach for the treatment of cerebral edema based on electroosmotic principle has been verified, showing the capability of directing edematous fluid at an acceptable velocity along electric current pathways from anode to cathode. The activated regions by the direct current are mainly observed between anode and cathode in which a faster EOF is induced. This approach is applicable for severe edema patients with DC, also could serve as a noninvasive complement for mild edema treatment.

Acknowledgment

The authors would like to thank the three anonymous reviewers and the editor for their stimulating comments and valuable suggestions that have substantially improved this paper.

References

[1] J. J. Donkin and R. Vink, "Mechanisms of cerebral edema in traumatic brain injury: Therapeutic developments," *Curr. Opin. Neurol.*, vol. 23, no. 3, pp. 293–299, 2010.

[2] B. P. Walcott *et al.*, "Novel treatment targets for cerebral edema," *Neurotherapeutics*, vol. 9, no. 1, pp. 65–72, 2012.

[3] H.-J. Feickert *et al.*, "Severe head injury in children: Impact of risk factors on outcome," *J. Trauma Acute Care Surg.*, vol. 47, no. 1, pp. 33–38, 1999.

[4] A. Marmarou, *Pathophysiology of Traumatic Brain Edema: Current Concepts*," Brain Edema XII: Springer, pp. 7–10, 2003.

[5] J. A. Kølsen-Petersen, "Osmotherapy," in *Management of Severe Traumatic Brain Injury: Evidence, Tricks, and Pitfalls,* New York, NY, USA; Berlin: Springer International Publishing, pp. 437–447, 2020.

[6] X. Li *et al.*, "Decompressive craniectomy causes a significant strain increase in axonal fiber tracts," *J. Clin. Neurosci.*, vol. 20, no. 4, pp. 509–513, 2013.

[7] D. J. Cooper *et al.*, "Decompressive craniectomy in diffuse traumatic brain injury," *N. Engl. J. Med.*, vol. 364, no. 16, pp. 1493–1502, 2011.

[8] G. M. Noetscher *et al.*, "Comparison of cephalic and extracephalic montages for transcranial direct current stimulation—A numerical study," *IEEE. Trans. Biomed. Eng.*, vol. 61, no. 9, pp. 2488–2498, 2014.

[9] S.-C. Bao *et al.*, "Cortico-muscular coherence modulated by high-definition transcranial direct current stimulation in people with chronic stroke," *IEEE Trans. Neural Syst. Rehabil. Eng.*, vol. 27, no. 2, pp. 304–313, Dec. 2018.

[10] M. Parazzini *et al.*, "A computational model of the electric field distribution due to regional personalized or nonpersonalized electrodes to select transcranial electric stimulation target," *IEEE. Trans. Biomed. Eng.*, vol. 64, no. 1, pp. 184–195, Jan. 2016.

[11] F. E. LeBeau *et al.*, "Iontophoresis in vivo demonstrates a key role for GABAA and glycinergic inhibition in shaping frequency response areas in the inferior colliculus of guinea pig," *J. Neurosci.*, vol. 21, no. 18, pp. 7303–7312, 2001.

[12] E. N. Lerner *et al.*, "Enhanced delivery of octreotide to the brain via transnasal iontophoretic administration," *J. Drug Target*, vol. 12, no. 5, pp. 273–280, 2004.

[13] A. H. Faraji *et al.*, "Electrokinetic convection-enhanced delivery of solutes to the brain," *ACS Chem. Neurosci.*, vol. 11, no. 14, pp. 2085–2093, 2020.

[14] A. H. Faraji *et al.*, "Electrokinetic infusions into hydrogels and brain tissue: Control of direction and magnitude of solute delivery," *J. Neurosci. Methods*, vol. 311, pp. 76–82, 2019.

[15] R. F. Probstein, *Physicochemical Hydrodynamics: An Introduction*, Hoboken, NJ, USA: John Wiley & Sons, 2005, pp. 26–40.

[16] L. P. Savtchenko *et al.*, "Electrodiffusion phenomena in neuroscience: A neglected companion," *Nat. Rev. Neurosci.*, vol. 18, no. 10, pp. 598–612, 2017.

[17] A. E. Hamsher *et al.*, "Minimizing tissue damage in electroosmotic sampling," *Anal. Chem.*, vol. 82, no. 15, pp. 6370–6376, 2010.

[18] Y. Ou and S. G. Weber, "Higher aminopeptidase activity determined by electroosmotic push–pull perfusion contributes to selective vulnerability of the hippocampal CA1 region to oxygen glucose deprivation," *ACS Chem. Neurosci.*, vol. 9, no. 3, pp. 535–544, 2017.

[19] Y. Ou *et al.*, "Electroosmotic perfusion of tissue: Sampling the extracellular space and quantitative assessment of membrane-bound enzyme activity in organotypic hippocampal slice cultures," *Anal. Bioanal. Chem.*, vol. 406, no. 26, pp. 6455–6468, 2014.

[20] A. E. Rupert *et al.*, "Electroosmotic push–pull perfusion: Description and application to qualitative analysis of the hydrolysis of exogenous galanin in organotypic hippocampal slice cultures," *ACS Chem. Neurosci.*, vol. 4, no. 5, pp. 838–848, 2013.

[21] A. Vijh, "Electrochemical field effects in biological materials: Electroosmotic dewatering of cancerous tissue as the mechanistic proposal for the electrochemical treatment of tumors," *J. Mater. Sci. Mater. Med.*, vol. 10, no. 7, pp. 419–423, 1999.

[22] Y. Guy *et al.*, "Determination of ζ-potential and tortuosity in rat organotypic hippocampal cultures from electroosmotic velocity measurements under feedback control," *Anal. Chem.*, vol. 81, no. 8, pp. 3001–3007, 2009.

[23] Y. Guy *et al.*, "Determination of ζ-potential in rat organotypic hippocampal cultures," *Biophys. J.*, vol. 94, no. 11, pp. 4561–4569, 2008.

[24] J. Wu *et al.*, "Integrated electroosmotic perfusion of tissue with online microfluidic analysis to track the metabolism of cystamine, pantethine, and coenzyme A," *Anal. Chem.*, vol. 85, no. 24, pp. 12020–12027, 2013.

[25] V. Fonov *et al.*, "Unbiased average age-appropriate atlases for pediatric studies," *Neuroimage*, vol. 54, no. 1, pp. 313–327, 2011.

[26] S. Pieper *et al.*, "3D Slicer," in *Proc. 2nd IEEE Int. Symp. Biomed. Imag.: Nano to Macro (IEEE Cat No. 04EX821)*, pp. 632–635, 2004.

[27] S. K. Boyd and R. Müller, "Smooth surface meshing for automated finite element model generation from 3D image data," *J. Biomech.*, vol. 39, no. 7, pp. 1287–1295, 2006.

[28] H. V. Helmholtz, "Studien über electrische grenzschichten," *Annalen der Physik*, vol. 243, no. 7, pp. 337–382, 1879.

[29] IT'IS Foundation, "Tissue properties database summary," [Online]. Available: https://itis.swiss/virtual-population/tissue-properties/database/database-summary
[30] A. Datta *et al.*, "Bio-heat transfer model of transcranial DC stimulation: Comparison of conventional pad versus ring electrode," in *Proc. Annu. Int. Conf. IEEE Eng. Med. Biol. Soc.*, pp. 670–673, 2009.
[31] M. M. Elwassif *et al.*, "Bio-heat transfer model of deep brain stimulation-induced temperature changes," *J. Neural. Eng.*, vol. 3, no. 4, pp. 306–315, 2006.
[32] S. B. Baumann *et al.*, "The electrical conductivity of human cerebrospinal fluid at body temperature," *IEEE. Trans. Biomed. Eng.*, vol. 44, no. 3, pp. 220–223, Mar. 1997.
[33] C. M. Collins *et al.*, "Model of local temperature changes in brain upon functional activation," *J. Appl. Physiol.*, vol. 97, no. 6, pp. 2051–2055, 2004.
[34] J. Haueisen *et al.*, "Influence of tissue resistivities on neuromagnetic fields and electric potentials studied with a finite element model of the head," *IEEE. Trans. Biomed. Eng.*, vol. 44, no. 8, pp. 727–735, 1997.
[35] M. M. de Oliveira *et al.*, "Heat transfer due to electroconvulsive therapy: Influence of anisotropic thermal and electrical skull conductivity," *Comput. Methods Programs Biomed.*, vol. 133, pp. 71–81, 2016, doi: 10.1016/j.cmpb.2016.05.022.
[36] D. Q. Truong *et al.*, "Computational modeling of transcranial direct current stimulation (tDCS) in obesity: Impact of head fat and dose guidelines," *Neuroimage. Clin.,* vol. 2, pp. 759–766, 2013.
[37] M. Akhtari *et al.*, "Conductivities of three-layer live human skull," *Brain Topogr.*, vol. 14, no. 3, pp. 151–167, 2002.
[38] E. Syková and C. Nicholson, "Diffusion in brain extracellular space," *Physiol. Rev.*, vol. 88, no. 4, pp. 1277–1340, 2008.
[39] Y. Huang *et al.*, "Measurements and models of electric fields in the in vivo human brain during transcranial electric stimulation," *Elife*, vol. 6, 2017, Art. no. e18834, doi: 10.7554/eLife.18834.001.
[40] S. Wagner *et al.*, "Investigation of tDCS volume conduction effects in a highly realistic head model," *J. Neural. Eng.*, vol. 11, no. 1, 2013, Art. no. 016002.
[41] H. von Holst *et al.*, "Increased strain levels and water content in brain tissue after decompressive craniotomy," *Acta Neurochir.*, vol. 154, no. 9, pp. 1583–1593, 2012.
[42] S. B. Ko *et al.*, "Real time estimation of brain water content in comatose patients," *Ann. Neurol.*, vol. 72, no. 3, pp. 344–350, 2012.
[43] E. B. Yan *et al.*, "Post-traumatic hypoxia exacerbates neurological deficit, neuroinflammation and cerebral metabolism in rats with diffuse traumatic brain injury," *J. Neuroinflamm.*, vol. 8, no. 1, pp. 1–16, 2011.
[44] J. Liu *et al.*, "Simultaneous detection of cerebral blood perfusion and cerebral edema using swept-source optical coherence tomography," *J. Biophoton.*, vol. 13, no. 2, 2020, Art. no. e201960087.
[45] H. Dafni *et al.*, "Overexpression of vascular endothelial growth factor 165 drives peritumor interstitial convection and induces lymphatic drain: Magnetic resonance imaging, confocal microscopy, and histological tracking of triple-labeled albumin," *Cancer Res.,* vol. 62, no. 22, pp. 6731–6739, 2002.
[46] L. M. Cancel *et al.*, "Direct current stimulation of endothelial monolayers induces a transient and reversible increase in transport due to the electroosmotic effect," *Sci. Rep.*, vol. 8, no. 1, pp. 1–13, 2018.
[47] S. Shahid *et al.*, "Numerical investigation of white matter anisotropic conductivity in defining current distribution under tDCS," *Comput. Methods Programs Biomed.*, vol. 109, no. 1, pp. 48–64, 2013.
[48] M. Bikson *et al.*, "Safety of transcranial direct current stimulation: Evidence based update," *Brain Stimul.,* vol. 9, no. 5, pp. 641–661, 2016.
[49] D. Liebetanz *et al.*, "Safety limits of cathodal transcranial direct current stimulation in rats," *Clin. Neurophysiol.*, vol. 120, no. 6, pp. 1161–1167, 2009.
[50] Y. Guy *et al.*, "Iontophoresis from a micropipet into a porous medium depends on the ζ-Potential of the medium," *Anal. Chem.*, vol. 84, no. 5, pp. 2179–2187, 2012.
[51] K. Nolkrantz *et al.*, "Electroporation of single cells and tissues with an electrolyte-filled capillary," *Anal. Chem.*, vol. 73, no. 18, pp. 4469–4477, 2001.
[52] M. A. Nitsche *et al.*, "Transcranial direct current stimulation: State of the art," *Brain Stimul,* vol. 1, no. 3, pp. 206–223, 2008.
[53] D. R. Merrill *et al.*, "Electrical stimulation of excitable tissue: Design of efficacious and safe protocols," *J. Neurosci. Methods*, vol. 141, no. 2, pp. 171–198, 2005.
[54] P. Minhas *et al.*, "Electrodes for high-definition transcutaneous DC stimulation for applications in drug delivery and electrotherapy, including tDCS," *J. Neurosci. Methods*, vol. 190, no. 2, pp. 188–197, 2010.
[55] E. A. Kiyatkin, "Brain hyperthermia during physiological and pathological conditions: Causes, mechanisms, and functional implications," *Curr. Neurovasc. Res.*, vol. 1, no. 1, pp. 77–90, 2004.